



Topological gelation of reconnecting polymers

Andrea Bonato^{a,1}, Davide Marenduzzo^a, Davide Michieletto^{a,b}, and Enzo Orlandini^{c,d}

Edited by Alexander Grosberg, New York University, New York, NY; received May 6, 2022; accepted September 27, 2022 by Editorial Board Member Paul Chaikin

DNA recombination is a ubiquitous process that ensures genetic diversity. Contrary to textbook pictures, DNA recombination, as well as generic DNA translocations, occurs in a confined and highly entangled environment. Inspired by this observation, here, we investigate a solution of semiflexible polymer rings undergoing generic cutting and reconnection operations under spherical confinement. Our setup may be realized using engineered DNA in the presence of recombinase proteins or by considering micelle-like components able to form living (or reversibly breakable) polymer rings. We find that in such systems, there is a topological gelation transition, which can be triggered by increasing either the stiffness or the concentration of the rings. Flexible or dilute polymers break into an ensemble of short, unlinked, and segregated rings, whereas sufficiently stiff or dense polymers self-assemble into a network of long, linked, and mixed loops, many of which are knotted. We predict that the two phases should behave qualitatively differently in elution experiments monitoring the escape dynamics from a permeabilized container. Besides shedding some light on the biophysics and topology of genomes undergoing DNA reconnection *in vivo*, our findings could be leveraged *in vitro* to design polymeric complex fluids—e.g., DNA-based complex fluids or living polymer networks—with desired topologies.

DNA topology | topological gel | living polymers | MD simulations

Recombination of genetic material involves the transient cleavage of two DNA segments that are spatially proximate in three dimensions (3D)—although not necessarily adjacent in one dimension—followed by alternative rejoining of DNA ends. Beyond its role in meiosis (1), similar topological processes involving the reconnection of DNA segments are also seen in the proliferation of transposable elements (2, 3) and the integration of viral DNA in the host genome (4). More recently, artificially driven DNA translocation- and recombination-like events have been used to map highly accessible genomic sites (5) and scramble synthetic yeast chromosomes (6). Recombination operations on a plasmid *in vitro* are known to yield linked or knotted DNA products (7–9). This observation suggests that unrestricted DNA recombination *in vivo* may pose a pressing topological problem to the cell (10, 11), but also that recombination may be employed to design topologically nontrivial DNA molecules.

Enzyme-mediated recombination has been well studied on short plasmids in dilute conditions (8, 12–15). On the other hand, the topological consequences of recombination operations on long and entangled DNA are far less investigated or understood. Inspired by this problem, here, we study a system of ring polymers continuously undergoing cutting and reconnection operations—hereafter called “reconnecting” or “recombinant” rings—inside a sphere (Fig. 1A). We note that, at variance with meiotic recombination, where two finite chromosome sections are exchanged, our reconnection operations are performed by introducing an exchange event on a single site, followed by alternative rejoining of the polymer segments (Fig. 1A). Therefore, our model entails a highly simplified view of recombination, and its aim is consequently limited to exploring the generic and qualitative topological feature of recombination in confinement, rather than making quantitative predictions. At the same time, our system can be viewed more generally as a confined melt of living polymer loops. Living polymers are reversibly breakable: Like the polymers in Fig. 1A, they can break and rejoin locally (i.e., reconnect), while remaining in thermal equilibrium (16). A melt of living polymer loops can form spontaneously following polymerization of monomers, given an appropriate choice of the reaction kinetics (17). As we discuss below, such melts can, in principle, be realized experimentally and, hence, are potentially relevant to materials science.

We discover that, depending on polymer stiffness and the radius of the confining sphere, these systems display a topological transition between a regime with many short, unlinked, and segregated rings and another one with few long, mixed, and linked rings. Geometrically, this transition is naturally explained as the result of a competition between bending energy of the loops and entropy of the system. Topologically, it can be seen

Significance

Shuffling of genetic material via reconnection of proximal DNA segments is seen in meiosis and some cancers. In contrast with textbook pictures, reconnections are performed within an entangled environment and can result in knotting or linking, detrimental for cells. By performing Brownian dynamics simulations of reconnecting polymers under confinement, modeling the genome *in vivo*, we find a topological transition between a gas or liquid of unlinked rings and a gel-like structure with a large number of polydisperse linked rings. This transition can be triggered by increasing polymer stiffness or confinement. Our results suggest ways to design future topological materials, such as DNA-based gels involving recombinase proteins.

Author affiliations: ^aSchool of Physics and Astronomy, University of Edinburgh, Edinburgh, EH9 3FD, United Kingdom; ^bMRC Human Genetics Unit, Institute of Genetics and Cancer, University of Edinburgh, Edinburgh EH4 2XU, United Kingdom; ^cDepartment of Physics and Astronomy, University of Padova, I-35131 Padova, Italy; and ^dSezione di Padova, Istituto Nazionale di Fisica Nucleare, I-35131 Padova, Italy

Author contributions: D. Marenduzzo, D. Michieletto, and E.O. designed research; A.B., D. Michieletto, and E.O. performed research; A.B. and E.O. analyzed data; and A.B., D. Marenduzzo, D. Michieletto, and E.O. wrote the paper.

The authors declare no competing interest.

This article is a PNAS Direct Submission. A.G. is a guest editor invited by the Editorial Board.

Copyright © 2022 the Author(s). Published by PNAS. This open access article is distributed under Creative Commons Attribution License 4.0 (CC BY).

¹To whom correspondence may be addressed. Email: andrea.bonato@strath.ac.uk.

This article contains supporting information online at <https://www.pnas.org/lookup/suppl/doi:10.1073/pnas.2207728119/-DCSupplemental>.

Published October 24, 2022.

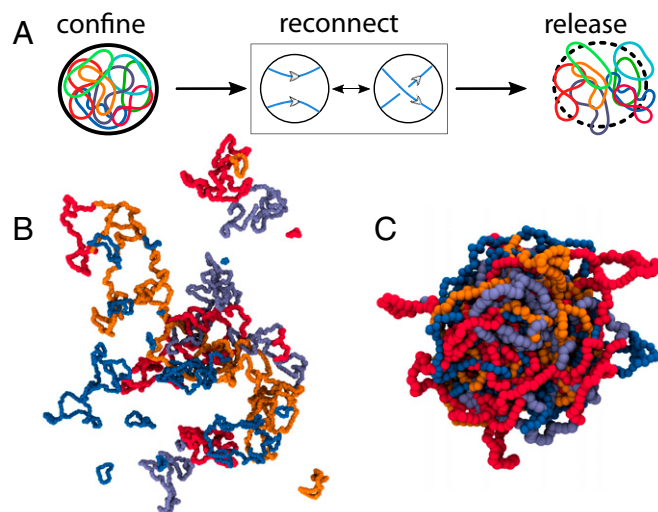


Fig. 1. Phases of reconnecting rings. (A) We study ring polymers allowed to recombine/reconnect within a sphere of radius R . (B and C) The two panels show two possible states of the system at equilibrium and after relaxing the confinement. *B* is a sketch of an ensemble of many, small, and mostly unlinked rings, whereas *C* shows an ensemble of few, long, and linked rings. The snapshots are taken after releasing confinement for ease of visualization.

as a gelation transition and understood in terms of the critical overlap concentration c^* , above which linking is expected to be entropically favored. Our gel of recombinant polymers is fundamentally different from other types of topological gels formed by nearly monodisperse loops in the presence of topoisomerase-like enzymes, such as the kinetoplast DNA network (18) or Olympic gels (19, 20), because in our case, multicomponent links are generically polydisperse and typically contain one or very few loops that are much longer than the rest and are often knotted. Similarly, our setup is distinct from that of previous works investigating the segregation of fixed-size polymer rings in a melt or under confinement (21–28) because the latter did not consider reconnection operations, which can change loop sizes and global topology.

The topological gelation we find in this work suggests that unregulated single-site reconnection of DNA *in vivo* should be highly detrimental. On the other hand, being able to construct a phase diagram for gelation *in vitro* can be useful from a materials-science perspective, as it may provide an avenue to design experiments with DNA rings, which undergo recombination under confinement to yield linked and knotted products with desired topologies or materials with topologically controlled mesoscopic properties—e.g., Olympic ring-like gels (19, 20).

A Model for Reconnecting Polymers

Unless otherwise specified, the system is initialized as one ring with $N = 1,000$ beads of size σ (see *SI Appendix* for results with $N = 10,000$). The beads interact via a purely repulsive Lennard-Jones potential, and adjacent beads are connected by finitely extensible nonlinear elastic bonds. A key parameter of our system is the stiffness, K , of the chains, which is proportional to the chain persistence length, imposed via a Kratky–Porod potential (29, 30) (*Materials and Methods*). The simulations are performed in LAMMPS (31) by using a Langevin thermostat and a time step $\Delta t = 0.001\tau_B$, with τ_B the Brownian time (see *SI Appendix* for more details). The polymer is initialized inside a large sphere that is slowly compressed to $R = 7\sigma$ and subsequently allowed to equilibrate. After this equilibration step, we allow the ring to undergo reconnections—i.e., transient single-site breakage

followed by alternative joining—between any two segments that are proximal in 3D (Fig. 1; effectively, we consider only segments closer than $r_c = 1.3\sigma$). Reconnection moves are attempted at every integration step (if the distance condition is satisfied) and are performed via a modified fix bond/swap (32–35) (*SI Appendix*). Since we accept or reject the moves according to a Metropolis test, the actual reconnection rates κ_r depend on the stiffness parameter K : for instance, $\kappa_r = 0.235\tau_B^{-1}$ at $K = 0$ and $\kappa_r = 0.004\tau_B^{-1}$ at $K = 5$. By mapping our Brownian time to real units (assuming $\sigma = 30$ nm and a medium with viscosity $\eta = 100$ cP as the nucleoplasm), these rates can be converted to 0.5 to 30 s^{-1} . These are overall faster than the 1/min recombination rates in biological systems (36), but of the same order as recombination in wormlike micelles (16, 37). Importantly, the precise value of κ_r does not affect our conclusions, as we are interested in the long-time, steady-state behavior of the system, rather than the transient dynamics.

Every $10^2\tau_B = 10^5\Delta t$, we take a snapshot of the system, reconstruct its topology, and record the chain number, $N_r(t)$, as well as their length distribution $L_r(n, t)$. The total number of beads in the system is kept constant to $N = 1,000 = \sum_{n=0}^{N_r(t)} L_r(n, t)$, so that the monomer density is $\rho = 3N/(4\pi R^3) \simeq 0.7\sigma^{-3}$ or, equivalently, the volume fraction $\phi = 0.37$. We have further checked that our system yields similar results with $N = 10,000$ beads and also starting from different initial conditions. For more details on our model, see *Materials and Methods* and *SI Appendix*.

Results

Geometry of Confined Reconnecting Rings. We begin by characterizing the geometrical features of the system as a function of the stiffness parameter K (proportional to the persistence length of the rings, l_p) for a fixed value of spherical confinement R . We monitor the average number of rings and their average length: In our simulations, both these quantities evolve to reach a well-defined steady-state value (Fig. 2 *A* and *B*).

Our data are suggestive of a smooth transition or cross-over between a regime in which many short rings populate the sphere (at low stiffness K) and another one in which few long rings remain in steady state (at high stiffness K). We temporarily refer to these as the short-ring and the long-ring regimes, respectively. A typical snapshot of the system in the two regimes is shown in Fig. 1 *B* and *C* (where the confining sphere is removed for ease of visualization). The transition can be understood in terms of the competition between the bending energy of the loops—regulated by K , which favors the long-ring regime—and their combinatorial and translational entropy—which favors the short-ring regime. To estimate entropy, we note that if we allow all rings to freely reconnect, the number of ways in which N beads can be distributed into m rings (without leaving any one of these empty) is given by the Stirling number of the second kind $\{N, m\} \sim m^N/m!$ for large N . Including the bending energy as well as the configurational entropy of rings (see *SI Appendix* for details), the total free energy of the system—apart from an irrelevant additive constant—can be estimated as

$$\frac{F}{k_B T} = \frac{2l_p\lambda\pi^2 m^2}{L} + m \log m - m - m \log aV, \quad [1]$$

with λ a numerical factor related to the specific shape taken by a curved polymer and a a numerical factor specified in *SI Appendix*.

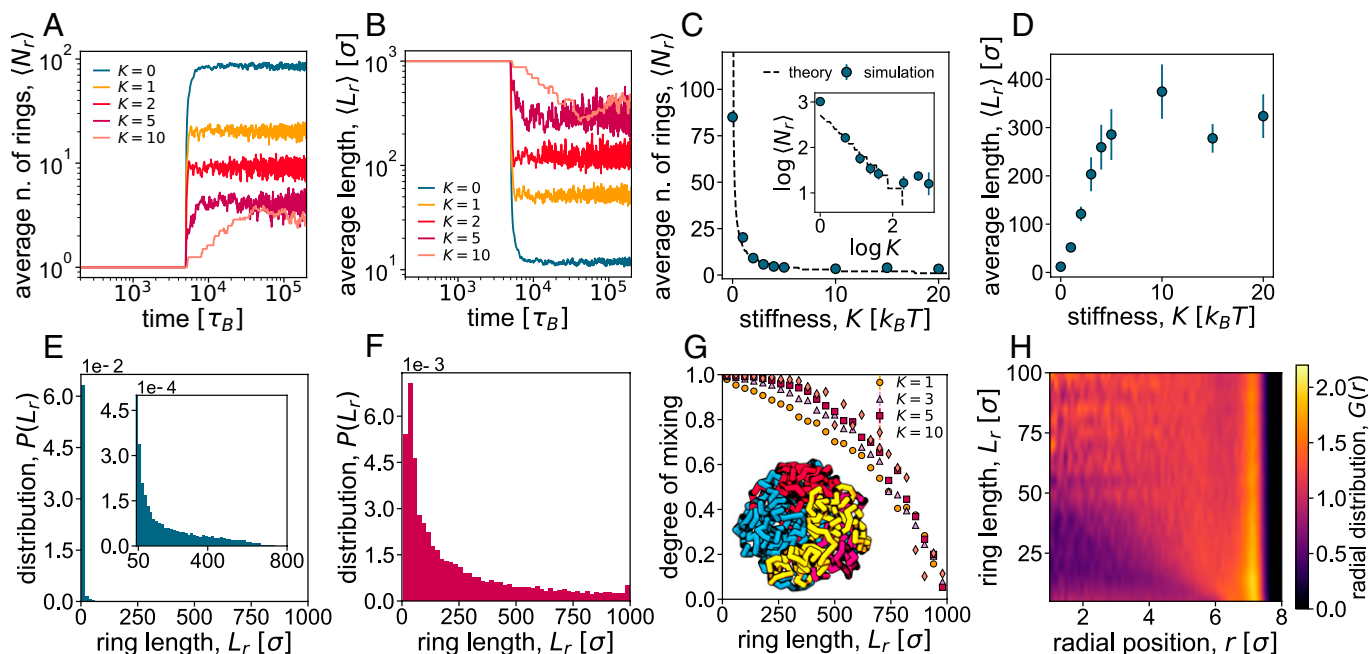


Fig. 2. Geometrical transition of reconnecting rings. (A and B) Time evolution of the average number (n.) of reconnecting rings N_r (A) and their average contour length L_r (B). Different curves refer to different values of the stiffness parameter K . All the data refer to a spherical confinement of radius $R = 7\sigma$. (C and D) Average steady-state values of $\langle N_r \rangle$ and $\langle L_r \rangle$, respectively, as a function of K . The black line in C and D, Inset shows the theoretical prediction from Eq. 1 with $\lambda = 5.3$ and $\alpha = 0.27$. (E and F) Distributions of ring size in steady state, for $K = 1$ (E) and $K = 5$ (F), indicating that the system is always highly polydisperse. (G) Probability that a ring of length L_r mixes with other rings as a function of L_r , for different values of K . (H) Heatmap of the radial distribution ($G(r)$) of monomers in rings of length L_r as a function of r , the distance from the center of the confinement sphere, and L_r .

We note that we assumed the curvature to scale as $\sim 1/L$, which is valid for short rings such that $L \simeq ml_p$; we shall see below that this assumption holds for our system.

By minimizing the free energy with respect to m , we can find the average number of rings as a function of K and R . As seen in Fig. 2C (and Fig. 2C, Inset), this mean-field theory captures the numerical results for the average number of rings, $\langle N_r \rangle$, very accurately. In particular, both our simulations and our theory predict that $\langle N_r \rangle \sim K^{-1}$. Eq. 1 also naturally describes the behavior of the expected mean length $\langle L_r \rangle$, thanks to the fact that the total number of monomers is conserved. As shown in Fig. 2D, the mean length displays a smooth transition, reaching a plateau at large values of K . Therefore, our theory shows that increasing K leads to a transition (or cross-over) between the short-ring and the long-ring regimes. In SI Appendix, we give more details about our semianalytical theory and show that a similar transition can be observed at fixed stiffness K by decreasing the sphere radius R (SI Appendix, Fig. S1).

An intriguing feature of our reconnecting polymer system is that the rings obtained in steady state have a very broad size distributions (Fig. 2E and F and SI Appendix, Figs. S2 and S3). Notably, this is true for both small and large K , and the size distribution is a power law, $P(L_r) \sim 1/L_r$, for all cases (SI Appendix, Fig. S2). As reconnection changes polymer length, but does not violate detailed balance in our model, the system is effectively in thermodynamic equilibrium, and the size distribution should be linked to the Boltzmann weight of rings of different sizes. Neglecting the dependence on K , which is expected to be a fair approximation for sufficiently long rings, we therefore expect the size distribution to be $\sim L_r^{-c}$ —i.e., the probability of forming a loop of size L_r . We note that a power-law size distribution of rings is also found, for analogous reasons, in living (reversibly breakable) polymers in the phase where loops are favored over linear chains (17). As discussed in more detail later, the inherent polydispersity of reconnecting

rings plays an important role to determine the emerging macroscopic properties of our system.

Radial Positioning and Mixing of Reconnecting Rings. In vivo, chromosomes segregate into territories, which position themselves nonrandomly with respect to the nuclear lamina. In this process, entropic effects play an important role (38, 39). Motivated by this, we ask how entropy and stiffness affect mixing and nonrandom positioning of reconnecting rings (which may be viewed as toy chromosomes) inside the sphere (a toy nucleus).

To this end, we construct a parameter, similar to the conditional entropy used to measure the entropy of mixing (40, 41), which quantifies the probability of finding monomers from other rings within a sphere centered at a monomer in a given ring. In Fig. 2G, we show that this mixing probability decreases with ring length and increases with stiffness K , as expected for concentrated solutions (42). In other words, longer and more flexible rings are less mixed. To further characterize the spatial arrangement of the rings, we compute the normalized radial density of monomers, $G(r)$ (Fig. 2H and SI Appendix, Fig. S4). Uniform positioning of beads, and hence of rings, within the sphere corresponds to a constant $G(r)$. Instead, we see that smaller loops (small L_r) are depleted in the interior of the sphere and enriched at the periphery $r \simeq 7\sigma$ (Fig. 2H and SI Appendix, Fig. S5). This is a consequence of steric depletion (43) and geometry, as smaller soft objects can approach a surface more frequently than larger ones. This finding also suggests that smaller plasmids or extrachromosomal DNA may be found more frequently toward the periphery of the cell (in bacteria) or nucleus (in eukaryotes).

The Short- and Long-Ring Phases are Separated by a Topological Gelation Transition. Up to now, we have shown that increasing the stiffness K in a melt of reconnecting rings drives a transition or cross-over between a short-ring and a long-ring regime. As anticipated, and as shown in SI Appendix, the same transition

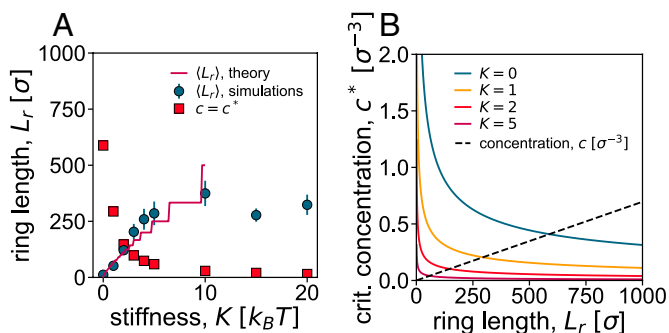


Fig. 3. Critical point for gelation. (A) Filled squares: critical length L^* , for which the concentration c of a ring in a sphere with $R = 7\sigma$ equals c^* , as a function of K . Filled circles: mean ring length versus K . The critical point for gelation is expected to be where the two curves cross. (B) Calculation of L^* . At L^* , the curves (c^* as a function of K) and the dotted line (c as a function of K) intersect. c^* is predicted for an ideal polymer ring (Eq. 2). Crit., critical.

or cross-over can also be achieved by increasing the ring density at a fixed value of the stiffness. More insight into this transition, and its underlying physical mechanism, can be gained by analyzing the overlap between reconnecting rings of different stiffness. For increasing values of stiffness, the average length of the rings in steady state is larger (Fig. 3A; blue circles are the same as in Fig. 2D), in turn entailing more overlaps. Calling L the average length of the rings, we can define a critical overlap concentration as

$$c^* = \frac{3L}{4\pi\sigma R_g^3}, \quad [2]$$

with R_g the radius of gyration of the rings. This is the concentration above which rings of size L start to overlap with each other. For our case, assuming that $R_g^2 = (L/2l_p)(2l_p)^2/12$ for $K \geq 1$ and that $R_g^2 = L\sigma/12$ for $K = 0$, we find c^* as a function of L (Fig. 3B). Using this curve, we can predict the critical value of the length for which $c = c^*$ as a function of stiffness, in turn, yielding the red curve in Fig. 3A. This curve is a decreasing function of K ; in other words, increasing K makes it easier for rings to feel and overlap with each other.

Importantly, as a consequence of the opposing dependencies of the average ring length and of the critical overlapping length as a function of K , there is a point at which the two curves cross (Fig. 3A). The crossing point marks the critical point separating the short-ring from the long-ring regime. In more detail, when the red curve (filled squares) in Fig. 3A is above the blue curve (filled circles), then $c < c^*$, and we expect that rings should not overlap and therefore segregate, leading to the short-ring phase (Fig. 1B). Instead, when the red curve is below the blue one, then $c > c^*$, and we expect rings to mix and reconnect significantly with each other, leading to the long-ring phase (Fig. 1C). This reasoning suggests that the transition we observe is akin to a gelation transition, where rings can be seen as soft particles, which start to interact once c/c^* becomes large enough. It is indeed natural to expect that the system should behave as a gas or liquid of soft particles (the rings) for $c < c^*$ and as a gel (or a solid-like structure) for c sufficiently larger than c^* . The main difference with respect to colloidal gels of soft particles is that, in our case, there are no direct attractive interactions between rings. However, we expect topological interactions to be present, as above c^* , rings can link with each other, as occurs in concentrated solutions of fixed-size crossable rings (44). For this reason, we refer to the transition between the short- and long-ring phases as “topological gelation,” and we shall reinforce this interpretation in the analysis described in the following sections. We note that in our system,

increasing K leads to a decrease in c^* , whereas a decrease in R leads to an increase in c . This is why the system can be made to gel either by increasing K (Fig. 3) or by decreasing R because both of these variations increase the value of c/c^* and, hence, favor the gel phase.

We note that, for $K = 5$, an isotropic-to-nematic transition is expected around monomer density $\rho = 0.85\sigma^{-3}$ (29, 30), which is larger than the monomer density at which we work, at $\rho = 0.7\sigma^{-3}$. While alignment effects may be important, we argue that the main role in driving the topological transition is played by the overlap concentration c^* , as explained above. In line with this, in *SI Appendix*, we show that a similar unlinked-to-linked transition is observed for fully flexible ($K = 1$) chains, albeit at larger densities, $\rho \simeq 0.76\sigma^{-3}$.

Topological Gelation Is Accompanied by the Formation of a Percolating Network of Linked Loops. We now discuss in more depth the topological nature of the gelation transition between the short- and long-ring phases. To quantify the topological entanglement between the rings in the system, we first compute the Gauss linking number (*Materials and Methods*). We find that, as the reconnecting rings get stiffer, the typical topologies found at fixed confinement radius R are markedly different. Fig. 4 A and B show the time dependence of the number of linked pairs and of $\langle |Lk| \rangle$, the total absolute value of the linking number (see *Materials and Methods* and *SI Appendix* for its precise definition). These curves, and the steady-state averages plotted in Fig. 4 C and D, show that both of these quantities increase with the stiffness K , as expected from our argument that the short- to long-ring transition is akin to gelation (Fig. 3). Flexible rings are therefore typically short and unlinked, whereas stiffer loops are typically longer and linked (see *SI Appendix*, Fig. S6 for the $\langle |Lk| \rangle$ distribution). The transition or cross-over that we observe by increasing stiffness is thus associated with an increase in topological entanglement and in linking between chains. In keeping with our interpretation of the long-ring phase as a gel, we expect that the topological entanglement between rings should endow our system with a nonzero elastic modulus.

As topological gelation is approached, the nature of the typical network of linked rings forming in steady state changes qualitatively, as shown in Fig. 4 E and F. For low K (in the liquid phase), the network has low connectivity, and clusters have typically one or very few nodes (Fig. 4E). In sharp contrast, for large K (in the gel phase), there is a large connected component that accounts for a substantial fraction of all rings (Fig. 4F). More precisely, we can quantify topological gelation by measuring the probability that the network condenses into a single connected cluster of nodes, which appears to depart from zero abruptly at a critical value of K (Fig. 4F). From Fig. 4 E and F, one can appreciate a dramatic step-wise change at the critical value $K \simeq 2$, which is where $c/c^* \simeq 1$, according to our theory (Fig. 3A). Gelation is therefore accompanied by a percolation transition in the network of linked rings. In our system, rings outside the largest connected component are typically unlinked, so that the average fraction of rings in the largest component is approximately equal to the linking probability for any ring in the network. Fig. 4F shows that gelation occurs when this linking probability proxy is about $1/2$; interestingly, this is equal to the bond-percolation threshold for the square lattice, but significantly higher than that of most standard 3D lattices.

Rings in Reconnecting Topological Gels Often Form Complex Knots. We now turn to a more detailed analysis of the topology of the gel phase, which, as we shall see, features some unique

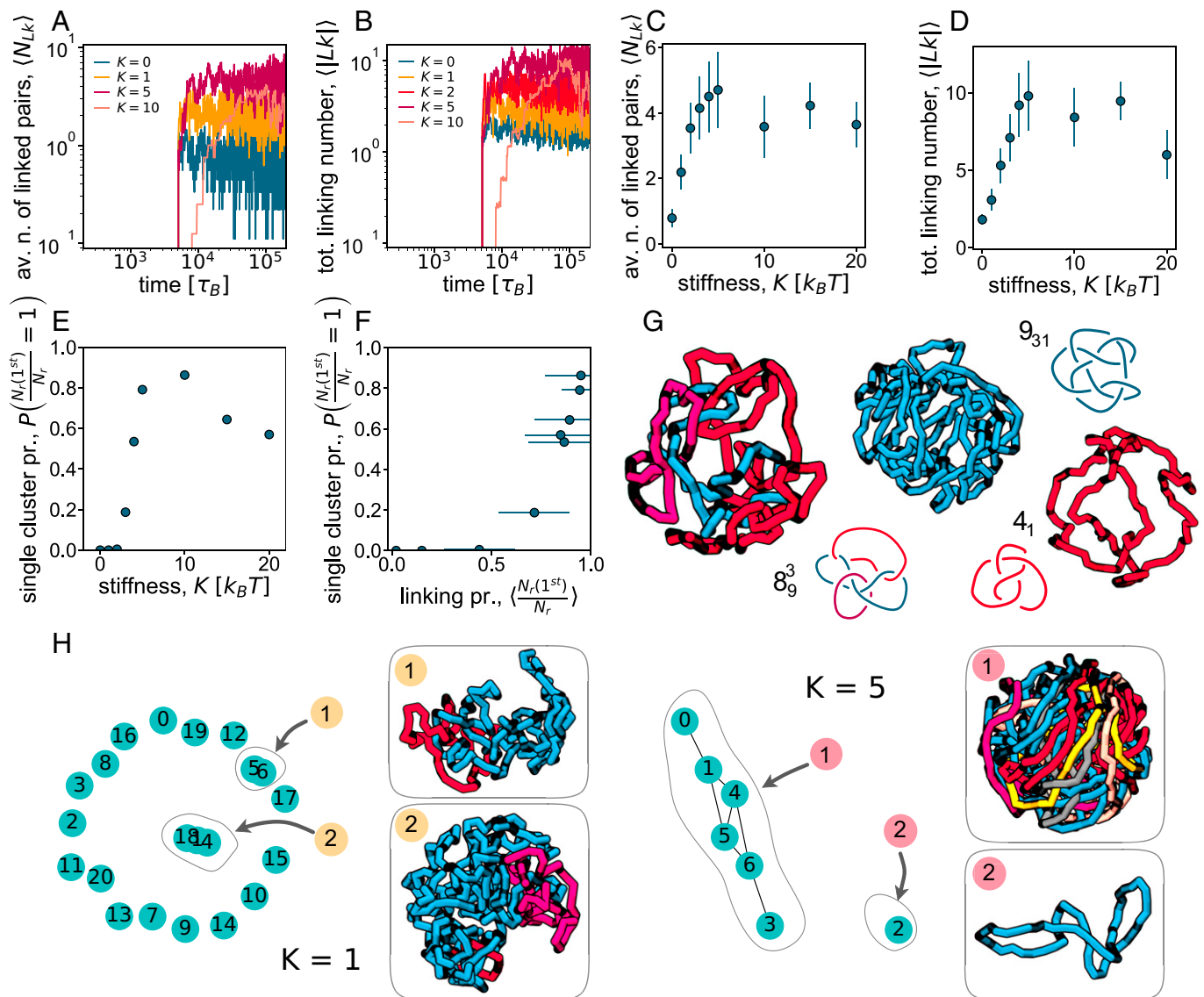


Fig. 4. Topological gelation. (A and B) Time dependence of the number of linked pairs of rings N_{Lk} (A) and average of the total unsigned linking number, $\langle |Lk| \rangle$, (B). Different curves refer to different values of the stiffness parameter K . (C and D) Average steady-state values of N_{Lk} and $\langle |Lk| \rangle$, respectively, as a function of K . (E and F) Probability of observing a single cluster as a function of K (E) and as a function of the linking probability (F). (G) Examples of knots and catenanes found in the steady-state configurations at $K = 5$. (H) Snapshots of clusters of linked rings in simulations with $K = 1$ and $K = 5$. Each sampled configuration is associated with a network; linked rings (vertices) are connected by edges. A connected component of the network represents a cluster of linked rings. Av., average; n., number; pr., probability; tot., total.

properties that cannot be found in topological gels with strand-crossing rings of fixed size. While classic Olympic gels (19, 20) are typically made by singly linked monodisperse rings [see also kinetoplast DNA (18, 44, 45)], topological gels from confined reconnecting rings possess much more complex and exotic structures (Fig. 4 G and H). First, recombination of rings can create knots, and, accordingly, we find that often, some rings in our gel phase are knotted. We typically observe that only the longest component in a link is knotted. Such knots can be relatively complicated—for instance, one of the two examples featured in Fig. 4G can be identified as a 9_{31} knot. Second, even unknotted rings may form complex catenanes: The one shown in Fig. 4G displays three rings that form an eight-crossing link (note that only two of the rings are pairwise linked, as a Solomon knot). Results for larger systems (where longer chains are confined in a larger sphere; *SI Appendix, Fig. S8*) are even more exotic. For instance, *SI Appendix, Fig. S8* shows a circular catenane and a 7_5 knot linked to two unknots in two different ways—as a Hopf

link with one and as a Solomon knot with the other. As found for the total linking number $\langle |Lk| \rangle$, we also observed that the complexity in topology tends to increase with K , or c/c^* , so that deeper in the gel phase, topologies are more complex than close to gelation.

How do such complex topologies form spontaneously through recombination/reconnection? We argue that this is due to the fact that the reconnection process allows ring length to vary. Indeed, in dilute conditions, multicomponent links made of equal-size rings that can exchange material are unstable for entropic reasons, and, as a result, one of the rings expands at the expense of all the others (46). Our results suggest that a similar entropic drive leads to the growth of a single ring in a multicomponent link also under confinement. Then, the larger ring is more likely to contain a knot, while the shorter rings are more likely to be unknotted; this is because knots have a statistical size that increases with their topological complexity (47). Clearly, this argument shows why topologies like those in Fig. 4H and *SI Appendix, Fig. S8* are

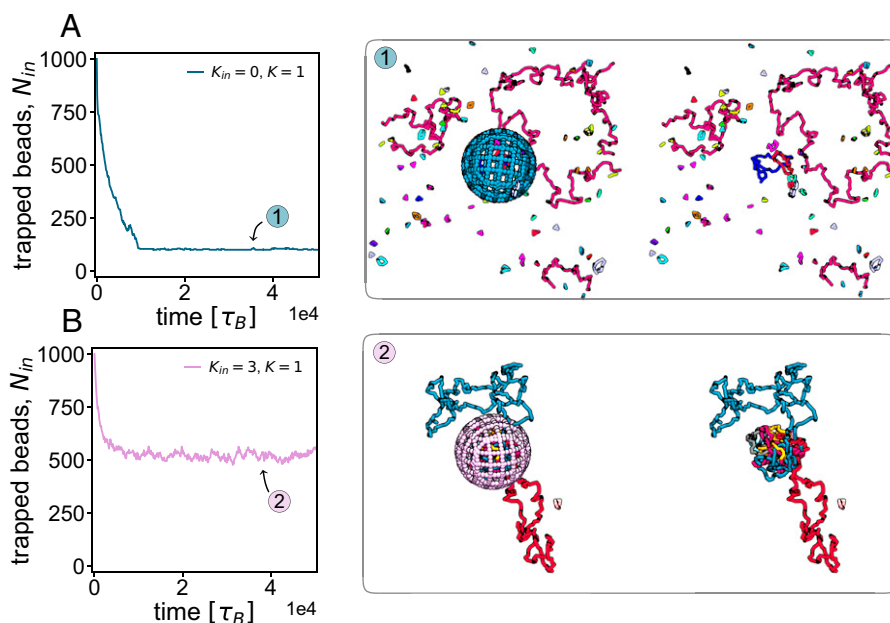


Fig. 5. Escape dynamics of reconnecting rings from a permeabilized sphere. Results of simulated elution experiments from a permeabilized sphere. The different structures correspond to a system of reconnecting rings with different K . After permeabilizing the sphere, K was set to 1 for all systems, and the reconnection was disallowed, in order to focus on the effect of topology on the escape dynamics. (Left) Number of monomers inside the sphere as a function of time for an initial value of K equal to 0 (A) and 3 (B). Corresponding snapshots are shown in Right (with and without the sphere to ease visualization of the topological structures). Simulations are performed inside a box with periodic boundaries.

impossible to obtain starting with monodisperse rings subject to strand-crossing moves, as these do not allow material exchange between rings.

Topological Gelation Traps the Reconnecting Rings Inside a Permeabilized Sphere. The topological transition we uncovered in the previous section can be vividly appreciated by the following procedure, which is inspired by elution experiments in biophysics and could, in principle, be realized in the laboratory (48). After a steady state is reached in our simulations, we permeabilize the confining sphere by converting it into a spherical mesh with pores of controlled size. We then disallow further reconnection and monitor the number of monomers still inside the sphere as a function of time, $n(t)$. The curves $n(t)$ are reported in Fig. 5 A and B for the liquid ($K = 0$) and gel ($K = 3$) regimes, respectively. It is apparent from the markedly different curves that the two regimes lead to very different escape dynamics. Note that, to single out the effect of the different topological states, after permeabilization, we set the stiffness to the same value ($K = 1$) in all cases.

In the liquid phase, the “dust” of overwhelmingly small and unlinked rings rapidly diffuses out of the sphere, as their translational entropy increases if confinement is removed, and such rings are small enough to translocate through the pores (snapshots in Fig. 5A). In this liquid or gas phase, longer rings, if present, are typically unlinked and can eventually exit the sphere. This behavior is qualitatively equivalent to that observed in experiments in permeabilized cells that show elution of sufficiently small molecules, such as diffusing proteins or DNA fragments of small size (48).

In sharp contrast, when the system is in the gel phase, the network of linked loops that emerges after reconnection is too large and topologically complex to translocate through the pores; most of the system is thus kinetically trapped inside the permeabilized sphere. This is apparent from the plateau of $n(t)$, suggesting a long-lived steady state with a substantial proportion of rings still inside the sphere (Fig. 5B). This second scenario is also

reminiscent of elution experiments, where large superstructures, like microphase-separated protein droplets or chromatin–protein aggregates, such as transcription factories, resist elution and remain inside the permeabilized nuclei (48).

In *SI Appendix*, we also consider the case where reconnections are still possible, and the stiffness is not reset, after permeabilization (*SI Appendix*, Fig. S9). This situation may correspond more closely to an actual experiment with confined living polymer rings. While the escape dynamics is, again, vastly different in the liquid and gel phases, in this case, all rings escape the sphere at small K , and the number inside the sphere decays as a stretched exponential. Instead, the behavior in the gel phase is very similar to that shown in Fig. 5, and the value of $n(t)$ reaches a nonzero plateau at large times.

Discussion and Conclusion

In summary, here, we have used coarse-grained molecular dynamics simulations to study the behavior of a solution of polymer rings undergoing recombination-like reactions (which we call reconnections; Fig. 1) inside a spherical container. There are two potential avenues to realize this system experimentally and to test our theoretical predictions *in vitro*. First, the system may be recreated by using a concentrated or confined mixture of suitably engineered DNA plasmids and recombinase enzymes. We note that a similar system was built to create synthetic scrambled yeast chromosomes (6). Second, one may use a confined ensemble of living ring polymers. The latter may be realized, for instance, by using fibril-forming proteins or patchy particles above the critical micellar concentration. As in wormlike micelles, rings are normally absent or irrelevant (16), it would be necessary to select proteins or particles whose geometry favors the formation of loops (49, 50). Additionally, the system we have considered here may be used as a very simplified framework to model the behavior of recombinant DNA *in vivo* [e.g., in the scrambled yeast chromosome system (6)].

Our main finding is that a confined solution of reconnecting polymer rings harbors a transition, or cross-over, between two fundamentally distinct regimes, which can be triggered either by stiffening the polymers or by increasing their density. For flexible or sufficiently dilute polymer rings, reconnection results in the production of a gas, or fluid, or short segregated and unlinked loops. For polymers with a sufficiently large persistence length, or for a sufficiently dense solution, a network of long linked loops emerges in steady state. This transition is a topological analog of the gelation transition observed for sufficiently dense suspensions of sticky colloids, where the formation of force chains is substituted by topological linking. Like gelation and vitrification, our topological transition is accompanied by a dramatic slowdown in the system dynamics, which could be quantified experimentally, for instance, by measuring the rate of escape from the confining sphere when the latter is pierced by appropriate-size pores to permeabilize it, as in elution experiments with DNA or chromatin. For large enough stiffness, our system is expected to undergo an isotropic-to-nematic transition involving spooling (51). Arguably, nematic alignment of polymer segments in this system may prevent proficient linking between different loops. Indeed, our simulations suggest that the onset of the topological gelation is mainly determined by the overlap concentration c^* , which depends on the equilibrium size of the polymer loops (itself dependent on the stiffness). Accordingly, in *SI Appendix*, we show that the unlinked–linked transition can be seen also for very flexible chains ($K = 1$) at large enough volume fractions.

The recombinant topological gel we have found here is fundamentally distinct from other topological gels obtained in DNA-ring solutions either in vitro or in vivo by using topoisomerase, such as Olympic gels (19, 20) or the kinetoplast DNA (18, 44, 45). In these two cases, DNA rings are monodisperse in length, typically unknotted and singly linked. In our recombinant gel, instead, rings are polydisperse, with a broad length distribution (*SI Appendix*, Fig. S2); they are also often knotted (*SI Appendix*, Fig. S10), especially at high concentrations, or under tight confinement. The difference between these two types of topological gels is inherently due to the difference between recombinase-like and topoisomerase-like operations, as the former does not need to preserve the ring lengths.

Besides being of fundamental interest as an example of a topological phase transition in a soft condensed-matter system, our results can therefore be exploited to design DNA gels with complex topologies. In this respect, it is important to note that topological (knot or link) complexity tends to increase with stiffness, or confinement, so that by selecting parameters appropriately, it should be possible to sieve networks with desired topologies. We anticipate that topological gelation can also be found if confinement is replaced by crowding—for instance, by varying the stiffness of a suspension of recombinant polymer loops of a sufficiently high-volume fraction. In such a geometry, the transition could be characterized, for instance, by measuring the bulk rheology response of the system, as the elastic modulus should be nonzero in the gel phase.

In the context of recombinant DNA in vivo, we speculate that our results suggest that recombination, when left unchecked, is likely to create a topological gel, given the high genomic density

found under physiological conditions in the nuclei of living cells. Gelation is likely detrimental for the cell, as it would lead to entanglements hindering, for instance, chromosome segregation during cell division. Interestingly, specific biological mechanisms, such as topoisomerase action and active chromosome movement, are indeed in place to remove chromosome interlocks (52–54), which are recombination-driven entanglements that form during early meiosis (55).

We hope that our work will inspire and inform future experiments on reconnecting DNA plasmids or living polymer rings at large density.

Materials and Methods

We simulate confined bead-spring polymers made of beads of size σ and mass m at a temperature T , inside a spherical container of radius R . The equations of motion, force fields, and the implementation of the reconnection moves are described in *SI Appendix*.

An attempted reconnection move, which would change the configuration of the system from ω to ω' (Fig. 1A and *A Model for Reconnecting Polymers*), is accepted with probability

$$p_{\text{swap}}(\omega', \omega) = \begin{cases} \exp(-\Delta E/k_B T) & \Delta E \geq 0 \\ 1 & \Delta E < 0, \end{cases} \quad [3]$$

where ΔE is the energy difference between ω and ω' .

The pairwise topological complexity of the system of rings is estimated by computing the Gaussian linking number for each pair of rings γ_i and γ_j , which is given by

$$Lk(\gamma_i, \gamma_j) = \frac{1}{4\pi} \oint_{\gamma_i} \oint_{\gamma_j} \frac{\mathbf{r}_1 - \mathbf{r}_2}{|\mathbf{r}_1 - \mathbf{r}_2|^3} \cdot (d\mathbf{r}_1 \times d\mathbf{r}_2). \quad [4]$$

For each pair (i, j) and sampling time t , we defined

$$\chi(i, j)(t) = \begin{cases} 1 & |Lk(\gamma_i, \gamma_j)|(t) > 0.5 \\ 0 & |Lk(\gamma_i, \gamma_j)|(t) \leq 0.5, \end{cases} \quad [5]$$

and, by summing over all pairs, we obtained the number of linked pairs of a given configuration at time t :

$$N_{lk}(t) = \frac{1}{2} \sum_{ij} N_r(t) \chi(i, j)(t), \quad [6]$$

where $N_r(t)$ is the number of rings at time t . The total absolute value of the linking number of a configuration is computed as

$$|Lk|(t) = \frac{1}{2} \sum_{ij} |Lk(\gamma_i, \gamma_j)|(t). \quad [7]$$

Different averages of N_{lk} and $|Lk|$ are shown in Fig. 4 A–D. Additional model details and supporting results are given in *SI Appendix*.

Data, Materials, and Software Availability. All study data are included in the article and/or supporting information. Data have also been deposited in GitLab, and are accessible at <https://git.ecdf.ed.ac.uk/taplab/topological-gelation> (56).

ACKNOWLEDGMENTS. D. Michieletto acknowledges the European Research Council (ERC) and Royal Society for funding. This project has received funding from the ERC under the European Union's Horizon 2020 research and innovation programme (grant agreement 947918, Topologically Active Polymers [TAP]).

1. B. Alberts, A. Johnson, J. Lewis, D. Morgan, M. Raff, *Molecular Biology of the Cell* (Taylor & Francis, Abingdon, UK, 2014).
2. B. Hallet, D. J. Sherratt, Transposition and site-specific recombination: Adapting DNA cut-and-paste mechanisms to a variety of genetic rearrangements. *FEMS Microbiol. Rev.* **21**, 157–178 (1997).
3. S. Pathania, M. Jayaram, R. M. Harshey, Path of DNA within the Mu transpososome. Transposase interactions bridging two Mu ends and the enhancer trap five DNA supercoils. *Cell* **109**, 425–436 (2002).

4. P. Sadowski, Site-specific recombinases: Changing partners and doing the twist. *J. Bacteriol.* **165**, 341–347 (1986).
5. J. D. Buenrostro, P. G. Giresi, L. C. Zaba, H. Y. Chang, W. J. Greenleaf, Transposition of native chromatin for fast and sensitive epigenomic profiling of open chromatin, DNA-binding proteins and nucleosome position. *Nat. Methods* **10**, 1213–1218 (2013).
6. Z. Luo et al., Identifying and characterizing SCRaMbLED synthetic yeast using ReScuES. *Nat. Commun.* **9**, 1930 (2018).

7. M. A. Krasnow *et al.*, Determination of the absolute handedness of knots and catenanes of DNA. *Nature* **304**, 559–560 (1983).
8. N. J. Crisona, R. L. Weinberg, B. J. Peter, D. W. Sumners, N. R. Cozzarelli, The topological mechanism of phage lambda integrase. *J. Mol. Biol.* **289**, 747–775 (1999).
9. S. A. Wasserman, N. R. Cozzarelli, Biochemical topology: Applications to DNA recombination and replication. *Science* **232**, 951–960 (1986).
10. J. M. Sogo *et al.*, Formation of knots in partially replicated DNA molecules. *J. Mol. Biol.* **286**, 637–643 (1999).
11. D. Goundaroulis, E. Lieberman Aiden, A. Stasiak, Chromatin is frequently unknotted at the megabase scale. *Biophys. J.* **118**, 2268–2279 (2020).
12. M. Vazquez, S. D. Colloms, D. Sumners, Tangle analysis of Xer recombination reveals only three solutions, all consistent with a single three-dimensional topological pathway. *J. Mol. Biol.* **346**, 493–504 (2005).
13. S. D. Colloms, J. Bath, D. J. Sherratt, Topological selectivity in Xer site-specific recombination. *Cell* **88**, 855–864 (1997).
14. S. C. Ip, M. Bregu, F. X. Barre, D. J. Sherratt, Decatenation of DNA circles by FtsK-dependent Xer site-specific recombination. *EMBO J.* **22**, 6399–6407 (2003).
15. F. J. Olorunniji *et al.*, Gated rotation mechanism of site-specific recombination by ϕ C31 integrase. *Proc. Natl. Acad. Sci. U.S.A.* **109**, 19661–19666 (2012).
16. M. Cates, Nonlinear viscoelasticity of wormlike micelles (and other reversibly breakable polymers). *J. Phys. Chem.* **94**, 371–375 (1990).
17. R. G. Petschek, P. Pfeuty, J. C. Wheeler, Equilibrium polymerization of chains and rings: A bicritical phenomenon. *Phys. Rev. A Gen. Phys.* **34**, 2391–2421 (1986).
18. J. Chen, C. A. Rauch, J. H. White, P. T. Englund, N. R. Cozzarelli, The topology of the kinetoplast DNA network. *Cell* **80**, 61–69 (1995).
19. E. Raphaël, C. Gay, P. De Gennes, Progressive construction of an “Olympic” gel. *J. Stat. Phys.* **89**, 111–118 (1997).
20. B. A. Krajina, A. Zhu, S. C. Heilshorn, A. J. Spakowitz, Active DNA Olympic hydrogels driven by topoisomerase activity. *Phys. Rev. Lett.* **121**, 148001 (2018).
21. Y. Jung *et al.*, Ring polymers as model bacterial chromosomes: Confinement, chain topology, single chain statistics, and how they interact. *Soft Matter* **8**, 2095–2102 (2012).
22. E. Minina, A. Arnold, Entropic segregation of ring polymers in cylindrical confinement. *Macromolecules* **48**, 4998–5005 (2015).
23. L. A. Mirny, The fractal globule as a model of chromatin architecture in the cell. *Chromosome Res.* **19**, 37–51 (2011).
24. A. Y. Grosberg, S. Nechaev, E. Shakhnovich, The role of topological constraints in the kinetics of collapse of macromolecules. *J. Phys. (Paris)* **49**, 2095–2100 (1988).
25. T. Vettorel, A. Y. Grosberg, K. Kremer, Statistics of polymer rings in the melt: A numerical simulation study. *Phys. Biol.* **6**, 025013 (2009).
26. J. D. Halverson, W. B. Lee, G. S. Grest, A. Y. Grosberg, K. Kremer, Molecular dynamics simulation study of nonconcatenated ring polymers in a melt. I. Statics. *J. Chem. Phys.* **134**, 204904 (2011).
27. H. Kang, Y. G. Yoon, D. Thirumalai, C. Hyeon, Confinement-induced glassy dynamics in a model for chromosome organization. *Phys. Rev. Lett.* **115**, 198102 (2015).
28. M. A. Ubertini, A. Rosa, Computer simulations of melts of ring polymers with nonconserved topology: A dynamic Monte Carlo lattice model. *Phys. Rev. E* **104**, 054503 (2021).
29. R. Faller, A. Kolb, F. Mu, Local chain ordering in amorphous polymer melts: Influence of chain stiffness. *Phys. Chem. Chem. Phys.* **1**, 2071–2076 (1999).
30. R. Faller, F. Müller-Plathe, A. Heuer, Local reorientation dynamics of semiflexible polymers in the melt. *Macromolecules* **33**, 6602–6610 (2000).
31. A. P. Thompson *et al.*, LAMMPS—A flexible simulation tool for particle-based materials modeling at the atomic, meso, and continuum scales. *Comput. Phys. Commun.* **271**, 108171 (2022).
32. N. C. Karayiannis, A. E. Giannousaki, V. G. Mavrantzas, D. N. Theodorou, Atomistic Monte Carlo simulation of strictly monodisperse long polyethylene melts through a generalized chain bridging algorithm. *J. Chem. Phys.* **117**, 5465–5479 (2002).
33. N. Ch. Karayiannis, V. G. Mavrantzas, D. N. Theodorou, A novel Monte Carlo scheme for the rapid equilibration of atomistic model polymer systems of precisely defined molecular architecture. *Phys. Rev. Lett.* **88**, 105503 (2002).
34. R. Auhl, R. Everaers, G. S. Grest, K. Kremer, S. J. Plimpton, Equilibration of long chain polymer melts in computer simulations. *J. Chem. Phys.* **119**, 12718–12728 (2003).
35. S. W. Sides, G. S. Grest, M. J. Stevens, S. J. Plimpton, Effect of end-tethered polymers on surface adhesion of glassy polymers. *J. Polym. Sci., B, Polym. Phys.* **42**, 199–208 (2004).
36. L. Ringrose *et al.*, Comparative kinetic analysis of FLP and Cre recombinases: Mathematical models for DNA binding and recombination. *J. Mol. Biol.* **284**, 363–384 (1998).
37. R. J. Hommel, M. D. Graham, Constitutive modeling of dilute wormlike micelle solutions: Shear-induced structure and transient dynamics. *J. Non-Newt. Fluid Mech.* **295**, 104606 (2021).
38. P. R. Cook, D. Marenduzzo, Entropic organization of interphase chromosomes. *J. Cell Biol.* **186**, 825–834 (2009).
39. D. Marenduzzo, E. Orlandini, Topological and entropic repulsion in biopolymers. *J. Stat. Mech. Theory Exp.* **2009**, L09002 (2009).
40. G. B. Brandani *et al.*, Quantifying disorder through conditional entropy: An application to fluid mixing. *PLoS One* **8**, e65617 (2013).
41. R. Fitzpatrick *et al.*, Synergistic interactions between DNA and actin trigger emergent viscoelastic behavior. *Phys. Rev. Lett.* **121**, 257801 (2018).
42. M. Bernabei, P. Bacova, A. J. Moreno, A. Narros, C. N. Likos, Fluids of semiflexible ring polymers: Effective potentials and clustering. *Soft Matter* **9**, 1287–1300 (2013).
43. S. Asakura, F. Oosawa, On interaction between two bodies immersed in a solution of macromolecules. *J. Chem. Phys.* **22**, 1255–1256 (1954).
44. D. Michieletto, D. Marenduzzo, E. Orlandini, Is the kinetoplast DNA a percolating network of linked rings at its critical point? *Phys. Biol.* **12**, 036001 (2015).
45. A. R. Klotz, B. W. Soh, P. S. Doyle, Equilibrium structure and deformation response of 2D kinetoplast sheets. *Proc. Natl. Acad. Sci. U.S.A.* **117**, 121–127 (2020).
46. A. Bonato, E. Orlandini, S. Whittington, Asymptotics of linked polygons. *J. Phys. A Math. Theor.* **53**, 385002 (2020).
47. V. Katritch, W. K. Olson, A. Vologodskii, J. Dubochet, A. Stasiak, Tightness of random knotting. *Phys. Rev. E Stat. Phys. Plasmas Fluids Relat. Interdiscip. Topics* **61** (5 Pt B), 5545–5549 (2000).
48. P. Hozák, A. B. Hassan, D. A. Jackson, P. R. Cook, Visualization of replication factories attached to nucleoskeleton. *Cell* **73**, 361–373 (1993).
49. J. M. Kalapothakis *et al.*, A kinetic study of ovalbumin fibril formation: The importance of fragmentation and end-joining. *Biophys. J.* **108**, 2300–2311 (2015).
50. G. Polles, D. Marenduzzo, E. Orlandini, C. Micheletti, Self-assembling knots of controlled topology by designing the geometry of patchy templates. *Nat. Commun.* **6**, 6423 (2015).
51. D. Marenduzzo, Statistics of confined polymers and the melting of a DNA spool. *EPL* **85**, 38005 (2009).
52. E. Piskadlo, R. A. Oliveira, A topology-centric view on mitotic chromosome architecture. *Int. J. Mol. Sci.* **18**, 1–21 (2017).
53. E. Orlandini, D. Marenduzzo, D. Michieletto, Synergy of topoisomerase and structural-maintenance-of-chromosomes proteins creates a universal pathway to simplify genome topology. *Proc. Natl. Acad. Sci. U.S.A.* **116**, 8149–8154 (2019).
54. S. Dyson, J. Segura, B. Martínez-García, A. Valdés, J. Roca, Condensin minimizes topoisomerase II-mediated entanglements of DNA in vivo. *EMBO J.* **40**, e105393 (2021).
55. M. Martínez-García *et al.*, TOP1 and chromosome movement help remove interlocks between entangled chromosomes during meiosis. *J. Cell Biol.* **217**, 4070–4079 (2018).
56. A. Bonato, D. Marenduzzo, D. Michieletto, E. Orlandini, Topological Gelation. *GitLab*. <https://git.ecdf.ed.ac.uk/taplab/topological-gelation>. Deposited 13 October 2022.